Optical Probes of Ultracold Neutral Plasmas

S. Laha, J. Castro, H. Gao, P. Gupta, C. E. Simien et al.

Citation: AIP Conf. Proc. **926**, 69 (2007); doi: 10.1063/1.2768834
View online: http://dx.doi.org/10.1063/1.2768834
View Table of Contents: http://proceedings.aip.org/dbt/dbt.jsp?KEY=APCPCS&Volume=926&Issue=1
Published by the American Institute of Physics.

Optical Probes of Ultracold Neutral Plasmas

S. Laha, J. Castro, H. Gao, P. Gupta, C. E. Simien, and T. C. Killian

Rice University, Department of Physics and Astronomy, Houston, Texas, 77005

Abstract. We describe the optical diagnostics used to study ultracold neutral plasmas. Imaging and spectroscopy based on both ion absorption and fluorescence provide accurate measurements of ion kinetic energy, plasma size, and the number of ions in the plasma. Absorption measurements yield lower signal-to-noise ratios because they are highly sensitive to laser intensity fluctuations, but the resulting measurement of the number of ions requires no external calibration. Fluorescence measurements of ion number must be calibrated with absorption measurements, but the measurements are less sensitive to technical noise sources. Spatially resolved fluorescence measurements also have the advantage of separating ion kinetic energy due to expansion from thermal kinetic energy.

Keywords: plasma imaging, laser cooling, strong coupling
PACS: 32.80.Pj,52.27.Gr

1. INTRODUCTION

Ultracold neutral plasmas are created by photoionizing laser-cooled atoms just above the ionization threshold [1]. In these systems, electrons have temperatures between 1 and 1000 kelvin, and ions equilibrate at about 1 kelvin. This represent an exotic regime of neutral plasma physics. At such low electron temperatures, processes such as three-body-recombination can be extremely fast [2, 3], and ions behave as a strongly-coupled fluid [4, 5, 6].

These experiments can teach us about plasmas across a much wider energy range. In particular, ultralow temperature allows experiments to access strongly-coupled physics at very low densities compared to high energy-density experiments. Because the densities are low, important time scales of the problem, such as the time between collisions and the inverse of the ion plasma oscillation frequency, are orders of magnitude longer, which greatly simplifies experiments. In addition, optical probes can precisely measure plasma properties, and ultracold plasmas have accurately known and controllable initial density profiles, energies, and ionization states.

In this paper, we will discuss the optical probes used to study ultracold neutral plasmas. In particular, spectroscopy and imaging based on plasma fluorescence is a new diagnostic that offers many powerful capabilities.

CP926, *Atomic Processes in Plasmas—15th International Conference on Atomic Processes in Plasmas*
edited by J. D. Gillaspy, J. J. Curry, and W. L. Wiese

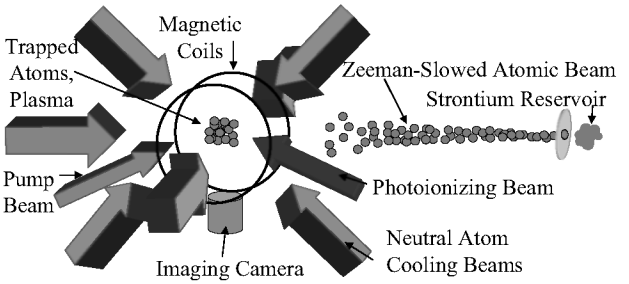

FIGURE 1. Schematic setup of a typical ultracold plasma experiment, exemplified with strontium atoms. Neutral atoms are laser cooled and trapped in a magneto-optical trap operating on the ${}^1S_0 - {}^1P_1$ transition at 461 nm, as described in [7]. In a second step, ${}^1P_1$ atoms are ionized by photons from a laser at ~ 412 nm (see Fig. 2A). Finally, the ionic plasma component is imaged using the ${}^2S_{1/2} - {}^2P_{1/2}$ transition in Sr^+ at 422 nm (see Fig. 2B). Probe beams for absorption and fluorescence follow different geometries and are not shown.

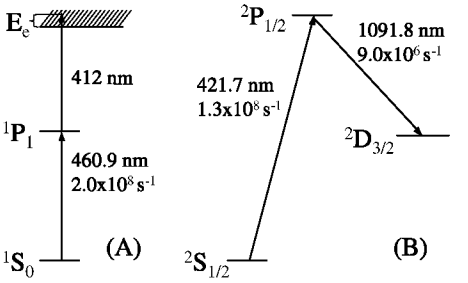

FIGURE 2. Strontium atomic and ionic energy levels with decay rates relevant for ultracold plasma experiments. (A) Creation of an ultracold plasma starts with laser cooling and trapping neutral atoms using the ${}^1S_0 - {}^1P_1$ transition at 461 nm. ${}^1P_1$ atoms are then photoionized with photons from a laser at ~ 412 nm. (B) Ions are optically imaged using the ${}^2S_{1/2} - {}^2P_{1/2}$ transition in Sr^+ at 422 nm. ${}^2P_{1/2}$ ions decay to the ${}^2D_{3/2}$ state 7% of the time, after which they cease to interact with the probe beam.

2. PLASMA CREATION

The creation of strontium ultracold neutral plasmas starts with laser-cooled neutral strontium. As described in [7], several hundred million strontium atoms are trapped in a magneto-optical trap (MOT) (Fig. 1) based on the ${}^1S_0 - {}^1P_1$ transition in Sr at 461 nm (Fig. 2A) and cooled to a temperature of a few mK. The atomic density distribution can be adjusted to have a spherical Gaussian form, $n_a(r) = n_a(0)\exp(-r^2/2\sigma^2)$, where the peak density for N_a atoms ($n_a(0) = N_a/(2\pi\sigma^2)^{3/2}$) is typically $10^{16}\,\mathrm{m}^{-3}$ and σ is typically 1 mm. The number of atoms and density of the cloud can be adjusted over several orders of magnitude by tuning the parameters

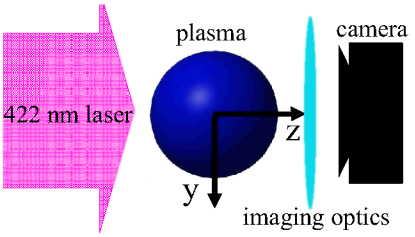

FIGURE 3. Absorption experimental layout. The absorption probe beam propagates along the $\hat{z}$-axis and falls on the camera. Absorption profiles are formed by recording an exposure with and without a plasma present, as described in the text. Spatial resolution can be utilized to isolate particular regions of the plasma, but all measurements integrate along the laser propagation direction.

of the lasers, magnetic fields, and atom-loading flux of the MOT.

Atoms are then photoionized in a two-photon process involving one 461 nm photon to promote atoms to the $^1P_1$ state and a 412 nm photon from a pulsed dye laser (~ 7 ns pulse) to promote electrons into the continuum. The plasma density profile follows the profile of the original laser-cooled atoms.

The ionization process adds energy to the electrons and ions, and the momentum change is negligible [8]. The electrons take away essentially all the excess photon energy as kinetic energy

$$E_e \approx h\nu_{ionize} - E_{IP} \tag{1}$$

where the ionization potential is E_{IP} and the 412 nm laser frequency is ν_{ionize}. The increase in ion kinetic energy is approximately $E_e m_e/m_i$, which is only on the order of mK even for $E_e = k_B 1000$ K. Within a few tens of nanoseconds after photoionization [9, 10], the electrons collisionally thermalize with themselves at $k_B T_e \approx 2E_e/3$. Establishment of local thermal equilibrium for the ions requires about $1\,\mu$s and displays characteristic behavior of strongly-coupled plasmas, such as disorder-induced heating [5, 11] and kinetic energy oscillations [12, 13].

3. ABSORPTION

Absorption by the ions of a near-resonant probe laser has proven to be a powerful diagnostic of ultracold plasmas that has been used to study disorder-induced heating of the ions [5], ion kinetic energy oscillations [12, 13], and plasma expansion [5, 14]. Strontium is a good choice for these experiments because absorption measurements can be performed using the Sr^+ $^2S_{1/2} \rightarrow {}^2P_{1/2}$ transition at 422 nm (Fig. 2B).

To measure the plasma absorption or optical depth, a collimated probe laser beam tuned near resonance with the principal transition in the ions (Fig. 2B) illuminates the plasma. Ions scatter photons out of the laser beam and create a shadow that is recorded by an image–intensified CCD camera (Fig. 3). The

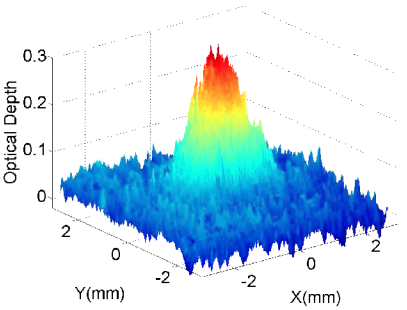

FIGURE 4. Optical depth measurement of a strontium ultracold neutral plasma. Reused with permission from [14]. Copyright 2004, Institute of Physics.

experimentally measured optical depth (OD) is defined in terms of the spatially resolved laser intensity without the plasma (I_0) and with the plasma present (I) as

$$OD(\nu, x, y) \quad = \quad \ln\left[I_0(\nu, x, y)/I(\nu, x, y)\right]. \tag{2}$$

Figure 4 shows a typical optical depth measurement. The delay between the formation of the plasma and camera exposure can be varied to study the time evolution of the plasma. Fast time resolution is obtained by gating the camera and the minimum camera exposure time is ~ 10 ns.

The typical absorption is a few percent at most. So the measurement is very sensitive to laser intensity-pattern fluctuations between the images with and without the plasma, which occur because of thermal effects in the nonlinear crystal used to generate the 422 nm light. This is the dominant source of noise and limits the practical regime of usefulness of the technique to plasmas with at least several tens of millions of ions and approximately the first $20\,\mu$s of plasma evolution.

3.1. Absorption Theory

Beer's law allows us to relate the OD theoretically to underlying physical parameters.

$$OD(\nu, x, y) \quad = \quad \int dz\, \rho_i(\mathbf{r}) \alpha[\nu, T_i(\mathbf{r}), \nu^z_{exp}(\mathbf{r})], \tag{3}$$

where $\rho_i(\mathbf{r})$ is the ion density, and $\alpha[\nu, T_i(\mathbf{r})]$ is the ion absorption cross section at the image beam frequency, ν. The absorption cross section is sensitive to random thermal ion motion and motion arising from plasma expansion because of Doppler broadening. The Doppler shift at $\mathbf{r}$ due to average expansion velocity $\mathbf{u}(\mathbf{r})$ is $\nu^z_{exp}(\mathbf{r}) = \mathbf{u}(\mathbf{r}) \cdot \hat{z}/\lambda$. The local ion temperature also varies with position $T_i = T_i(\mathbf{r})$.

The Voigt profile for the ion absorption cross section reads

$$\alpha(\nu, T_i, \nu^z_{exp}) = \int ds \frac{3^*\lambda^2}{2\pi} \frac{\gamma_0}{\gamma_{eff}} \frac{1}{1+4\left(\frac{\nu-s}{\gamma_{eff}/2\pi}\right)^2} \frac{1}{\sqrt{2\pi}\sigma_D(T_i)} \exp\left\{-\frac{[s-(\nu_0+\nu^z_{exp})]^2}{2\sigma_D(T_i)^2}\right\}, \quad (4)$$

where $\gamma_{eff} = \gamma_0 + \gamma_{ins}$ is the effective Lorentzian linewidth due to the natural linewidth $\gamma_0 = 2\pi \times 20\,\mathrm{MHz}$ of the transition and any instrumental linewidth γ_{ins}. The center frequency of the transition is $\nu_0 = c/\lambda$, and the "three-star" symbol [15] is a numerical factor that accounts for the polarization state of the ions and the imaging light. $\sigma_D(T) = \sqrt{k_B T/m_i}/\lambda$ is defined as is conventional for a Doppler width. We have neglected power broadening of the transition because the probe beam intensity of a few $\mathrm{mW/cm^2}$ is much less than the saturation intensity of the transition. The absorption can be analyzed in different ways that each explore different plasma properties.

3.2. Absorption Imaging

If Eq. 3 is integrated over frequency, the resulting expression is

$$\int d\nu\, OD(\nu, x, y) = \gamma_0 \frac{3^*\lambda^2}{8\pi} \int dz\, \rho_i(\mathbf{r}) \equiv \gamma_0 \frac{3^*\lambda^2}{8\pi} n_{areal}(x, y) \quad (5)$$

which gives a measure of the areal density, $n_{areal}(x, y)$. Experimentally, the integral is performed by summing a series of optical depth measurements taken at equally spaced frequencies that span the absorption resonance. The areal density can be integrated spatially to provide the ion number. Spatial dynamics of the plasma can be studied by recording images at different times.

3.3. Absorption Spectroscopy

The frequency dependence of the ion absorption can be found by integrating the optical depth measurement spatially,

$$S(\nu) = \int dx dy\, OD(\nu, x, y). \quad (6)$$

Experimentally, the camera pixels are summed. To analyze this data, Eq. 3 can be used to theoretically relate the frequency dependence of the ion absorption to the density weighted average of the absorption cross section

$$S(\nu) = \int d^3r\, \rho_i(\mathbf{r}) \alpha[\nu, T_i(\mathbf{r}), \nu^z_{exp}(\mathbf{r})]. \quad (7)$$

The camera's spatial resolution can be utilized to restrict the volume integral to a part of the plasma, and then the spectrum reflects the properties of the

plasma in that region. The variation with position of the Doppler broadening due to thermal motion and plasma expansion complicates Eq. 7, but to a good approximation [14], all Doppler-broadening can be described by introducing an effective ion temperature, which yields

$$S(\nu) = N_i \frac{3^*\lambda^2}{2\pi} \frac{\gamma_0}{\gamma_{eff}} \int ds \frac{1}{1+4\left(\frac{\nu-s}{\gamma_{eff}/2\pi}\right)^2} \frac{1}{\sqrt{2\pi}\sigma_D(T_{i,eff})} \exp\left[-\frac{(s-\nu_0)^2}{2\sigma_D(T_{i,eff})^2}\right]. \tag{8}$$

The effective Doppler width, $\sigma_D(T_{i,eff}) \equiv \sqrt{k_B T_{i,eff}/m_i}/\lambda$, which can be characterized by an effective temperature, measures the ion velocity along the laser propagation direction. For simple forms of the plasma expansion and $T_i(\mathbf{r})$, an analytic expression relates the velocity to time-varying plasma properties such as size, electron temperature, and ion temperature [8]. For a self-similar expansion and uniform ion temperature, $\sigma_D(T_{i,eff}) = \sqrt{[\langle(\mathbf{v}\cdot\hat{\mathbf{z}})^2\rangle]_{average}}/\lambda \equiv v_{i,rms}/\lambda$, where $\mathbf{v}$ is the total ion velocity including random thermal motion and expansion, the angled brackets refer to a local integral over the velocity distribution, and the average is over the plasma spatial distribution. In the absence of such simple conditions $\sigma_D(T_{i,eff}) \approx v_{i,rms}/\lambda$ is still a good approximation [14]. Absorption spectra fits also provide an absolute measure of the number of ions.

Fitting experimental absorption spectra to Eq. 8 provides a measure of the ion kinetic energy, but it is not possible to separate contributions from thermal motion and expansion. This restricts study of ion thermal properties using absorption to times less than a few microseconds, after which the expansion dominates the Doppler broadening [8].

4. FLUORESCENCE

Recent experiments have demonstrated the usefulness of fluorescence imaging and spectroscopy. It is intrinsically less sensitive to external noise, such as laser-power fluctuations, and thus is better-suited than absorption probes to study smaller plasmas or plasmas at long delays after formation. As shown below, it has the drawback of not providing an absolute measure of the number of ions in the plasma, so this technique works well in tandem with absorption diagnostics. In [6], monitoring the fluorescence level from a laser-beam focused in a small region of the plasma demonstrated some of the advantages of fluorescence as a probe, but imaging the fluorescence from excitation of the entire plasma provides much more information.

Figure 5 shows a schematic of the fluorescence experiment. A laser beam that is near resonance with the $^2S_{1/2} - {}^2P_{1/2}$ transition in Sr^+ at $\lambda = 422$ nm propagates along $\hat{y}$ and illuminates the plasma. Fluorescence in a perpendicular direction ($\hat{z}$) is recorded by the camera. A typical fluorescence measurement is also shown in Fig. 5. The 422 nm light is typically applied in a $2\,\mu$s pulse to provide temporal

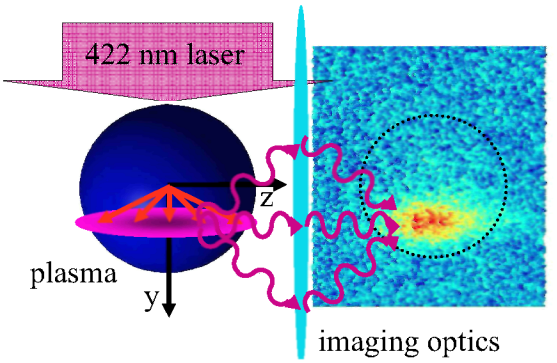

FIGURE 5. Recording fluorescence of UNPs. The correlation between position and expansion velocity (red arrows) produces a striped image when the Doppler-shift due to expansion exceeds the Doppler shift associated with thermal ion velocity.

resolution, and the intensity is only a few $\mathrm{mW/cm^2}$, which is low enough to avoid optical pumping to the metastable $^2D_{3/2}$ state.

4.1. Fluorescence Theory

By a procedure similar to the treatment of the absorption measurements, the fluorescence can be related to underlying physical parameters through

$$F(\nu,x,y) \propto \frac{\gamma_0}{2}\int \frac{dz\, n(\mathbf{r})I(\mathbf{r})/I_{sat}}{\sqrt{2\pi}\sigma_D[T_i(\mathbf{r})]}\int ds \frac{\gamma_0/\gamma_{eff}}{1+\left[\frac{2(\nu-s)}{\gamma_{eff}/2\pi}\right]^2}\exp\left\{-\frac{\left[s-(\nu_0+\nu^y_{exp}(\mathbf{r}))\right]^2}{2\sigma_D^2[T_i(\mathbf{r})]}\right\}, \tag{9}$$

where $I(\mathbf{r})$ is the intensity profile of the fluorescence excitation beam. We have neglected power broadening of the transition, so this expression is only valid for $I(\mathbf{r}) \ll I_{sat}$, where the saturation intensity for linearly polarized light, taking Clebsch-Gordon coefficients for the transition into account, is $I_{sat} = 114\,\mathrm{mW/cm^2}$. We have also omitted a multiplicative factor that depends upon collection solid angle, dipole radiation pattern orientation, and detector efficiency. This must be calibrated with absorption measurements in order to derive quantitative information from the amplitude of the signal.

It is important to note the form of the Doppler shift arising from expansion. Due to the directed expansion velocity, the average resonance frequency of the transition for atoms at $\mathbf{r}$ is Doppler-shifted from the value for an ion at rest, ν_0, by $\nu^y_{exp}(\mathbf{r}) = \mathbf{u}(\mathbf{r})\cdot\hat{y}/\lambda$. For most experimental conditions studied, the plasma expansion is self-similar [3, 9, 16], and $\mathbf{u}(\mathbf{r}) = \gamma(t)\mathbf{r}$, where γ depends upon the plasma parameters. So $\nu^y_{exp}(\mathbf{r}) = \gamma(t)y/\lambda$, which produces a correlation between

position in the camera and the Doppler shift due to expansion. This spatial shift allows the Doppler-effect contributions from expansion and thermal motion to be separated.

4.2. Fluorescence Imaging

As with absorption, fluorescence data can be analyzed in different ways, which each measure different plasma properties. Summing a series of camera exposures taken at equally spaced frequencies covering the entire ion resonance is equivalent to integrating Eq. 9 over frequency. This yields

$$\int d\nu\, F(\nu,x,y) \propto \int dz\, I(\mathbf{r}) n(\mathbf{r}). \tag{10}$$

If the plasma is much smaller than the laser beam waist, then the intensity variation is insignificant and an image of the plasma areal density is given by

$$\int d\nu\, F(\nu,x,y) \propto \int dz\, n(\mathbf{r}) = n_{areal}(x,y). \tag{11}$$

If the laser spatial variation cannot be neglected, it distorts the measurement of the plasma width along the $\hat{x}$-axis, but with knowledge of the laser waist size (w), the effect can be accounted for;

$$\begin{aligned} \int d\nu\, F(\nu,x,y) &\propto \int dz\, I_0 \exp\left(-\frac{2x^2+2z^2}{w^2}\right) n_0 \exp\left(-\frac{x^2+y^2+z^2}{2\sigma^2}\right) \\ &\propto \exp\left[-x^2\left(\frac{1}{2\sigma^2}+\frac{2}{w^2}\right)-\frac{y^2}{2\sigma^2}\right]. \end{aligned} \tag{12}$$

Figure 6 shows fluorescence images of an expanding plasma that show the effect of laser intensity variation.

4.3. Fluorescence Spectroscopy

If the laser intensity profile can be approximated as constant, the fluorescence signal can be interpreted as a spatially resolved light-scattering resonance spectrum. In practice, one integrates the signal over some region of the plasma,

$$\begin{aligned} \int_{reg} dxdy F(\nu,x,y) &\propto \int_{reg} dxdy \int \frac{dz\, n(\mathbf{r})}{\sqrt{2\pi}\sigma_D[T_i(\mathbf{r})]} \\ &\times \int ds \frac{\gamma_0/\gamma_{eff}}{1+\left[\frac{2(\nu-s)}{\gamma_{eff}/2\pi}\right]^2} \exp\left\{-\frac{\left[s-(\nu_0+\nu^y_{exp}(\mathbf{r}))\right]^2}{2\sigma_D^2[T_i(\mathbf{r})]}\right\} \\ &\approx N_{i,reg}\frac{1}{\sqrt{2\pi}\sigma_D[T_{i,reg}]} \int ds \frac{\gamma_0/\gamma_{eff}}{1+\left[\frac{2(\nu-s)}{\gamma_{eff}/2\pi}\right]^2} \exp\left\{-\frac{\left[s-(\nu_0+\nu^y_{exp,reg})\right]^2}{2\sigma_D^2[T_{i,reg}]}\right\}. \end{aligned} \tag{13}$$

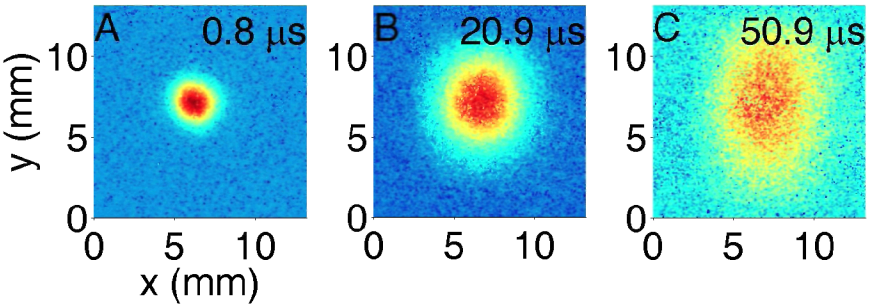

FIGURE 6. Fluorescence images showing expansion of the plasma. The indicated time is time after photoionization. In (A), the plasma is small enough that Eq. 11 is valid. By (C), the finite size of the fluorescence excitation laser elongates the plasma fluorescence even though the expansion is spherically symmetric. This distortion must be accounted for in order to accurately measure the areal density, as in Eq. 12.

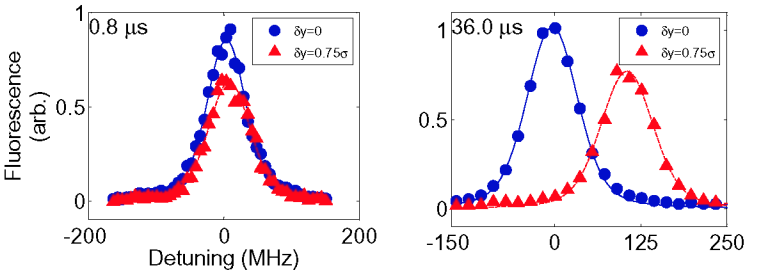

FIGURE 7. Fluorescence spectra of regions with little Doppler shift due to expansion ($\delta y = 0$) and significant Doppler shift ($\delta y = 0.75\sigma$) at two different times after photoionization. δy is the displacement along y of the region being analyzed (Eq. 13).

The z integral necessarily extends over the entire plasma, but $N_{i,reg}$ is the number of ions in the bounded $x-y$ region. $T_{i,reg}$ and $\nu^{y}_{exp,reg}$ are the average ion temperature and expansion-induced Doppler shift for the region. A typical fluorescence signal is so strong that the spatial extent of the region can be a small fraction of the length scale of variation of plasma properties (σ), so the average comes very close to a local value. It is important to note that this allows separation of the spectral influences of expansion and thermal motion because expansion leads to a shift in the spectrum, while thermal motion leads to a broadening. This is shown in Fig. 7.

5. CONCLUSIONS

We have described the optical diagnostics used to study ultracold neutral plasmas. Many of the experiments that have been performed with absorption measurements have been described previously, such as investigation of local thermal equilibration of strongly coupled ions [5, 12, 13], and plasm expansion at short times [5, 14]. Experiments are planned with fluorescence probes that will explore the establishment of global thermal equilibrium for ions and study the expansion dynamics over a longer time scale.

This work was supported by the National Science Foundation (Grant PHY-0355069) and the David and Lucille Packard Foundation.

REFERENCES

1. T. C. Killian, S. Kulin, S. D. Bergeson, L. A. Orozco, C. Orzel, and S. L. Rolston, *Phys. Rev. Lett.* **83**, 4776 (1999).
2. T. C. Killian, M. J. Lim, S. Kulin, R. Dumke, S. D. Bergeson, and S. L. Rolston, *Phys. Rev. Lett.* **86**, 3759 (2001).
3. F. Robicheaux, and J. D. Hanson, *Phys. Rev. Lett.* **88**, 55002 (2002).
4. S. Ichimuru, *Rev. Mod. Phys.* **54**, 1017 (1982).
5. C. E. Simien, Y. C. Chen, P. Gupta, S. Laha, Y. N. Martinez, P. G. Mickelson, S. B. Nagel, and T. C. Killian, *Phys. Rev. Lett.* **92**, 143001 (2004).
6. E. A. Cummings, J. E. Daily, D. S. Durfee, and S. D. Bergeson, *Phys. Rev. Lett* **95**, 235001 (2005).
7. S. B. Nagel, C. E. Simien, S. Laha, P. Gupta, V. S. Ashoka, and T. C. Killian, *Phys. Rev. A* **67**, 011401 (2003).
8. T. C. Killian, T. Pattard, T. Pohl, and J. M. Rost, submitted to *Physics Reports*, http://arxiv.org/abs/physics/0612097.
9. F. Robicheaux, and J. D. Hanson, *Phys. Plasmas* **10**, 2217 (2003).
10. L. Spitzer, Jr., *Physics of Fully Ionized Gases*, Wiley, New York, 1962.
11. M. S. Murillo, *Phys. Rev. Lett.* **87**, 115003 (2001).
12. Y. C. Chen, C. E. Simien, S. Laha, P. Gupta, Y. N. Martinez, P. G. Mickelson, S. B. Nagel, and T. C. Killian, *Phys. Rev. Lett.* **93**, 265003 (2004).
13. S. Laha, Y. C. Chen, P. Gupta, C. E. Simien, Y. N. Martinez, P. G. Mickelson, S. B. Nagel, and T. C. Killian, *Euro. Phys. J. D* **40**, 51 (2006).
14. T. C. Killian, Y. C. Chen, P. Gupta, S. Laha, Y. N. Martinez, P. G. Mickelson, S. B. Nagel, A. D. Saenz, and C. E. Simien, *J. Phys. B: At. Mol. Opt. Phys.* **38**, 351 (2005), (Equations 7, 10, 11, and 17 should be multiplied by γ_0/γ_{eff}.).
15. A. E. Siegman, *Lasers*, University Science Books, Sausolito, California, 1986.
16. T. Pohl, T. Pattard, and J. M. Rost, *Phys. Rev. A* **70**, 033416 (2004).